Solar Phys
DOI 10.1007/s11207-014-0526-6

RATAN-600 Observations of Small-Scale Structures with High Spectral Resolution

V.M. Bogod · C.E. Alissandrakis · T.I. Kaltman · S.K. Tokhchukova

Received: 22 November 2013 / Accepted: 27 March 2014

Abstract We present observations of quiet-Sun small-scale structures (SSS) in the microwave range with the *Radio Astronomical Telescope of the Academy of Sciences 600* (RATAN-600) spectral-polarization facility in a wide range of frequencies. The SSS are regularly recorded in routine observations of the large reflector-type radio telescope and represent manifestations in the radio range of various structures of the quiet Sun: supergranulation network, bright points, plage patches, and so on. A comparison with images from the *Solar Dynamics Observatory* (SDO) showed that the microwave emission comes from a region extending from the chromosphere to the low transition region. We measured the properties of the SSS as well as the degree of circular polarization averaged over the beam of the radio telescope, and from this we estimated the magnetic field at the formation level of the radiation.

Keywords Radio emission, quiet · Polarization, radio · Magnetic fields, chromosphere · Chromosphere, quiet · Transition region · Corona, quiet

New eyes looking at solar activity: Challenges for theory and simulations.
Guest Editors: Silja Pohjolainen and Marian Karlický

V.M. Bogod · T.I. Kaltman · S.K. Tokhchukova
St. Petersburg Branch, Special Astrophysical Observatory, Russian Academy of Sciences,
St. Petersburg, 196140, Russia

V.M. Bogod
e-mail: vbog_spb@mail.ru

V.M. Bogod
St Petersburg National Research University ITMO, St. Petersburg, Russia

C.E. Alissandrakis (✉)
Section of Astro-Geophysics, Department of Physics, University of Ioannina, 45110 Ioannina, Greece
e-mail: calissan@cc.uoi.gr

Published online: 18 April 2014

1. Introduction

The microwave range is rich in information on quiet-Sun structures in the upper chromosphere, the transition region, and the low corona (see Shibasaki, Alissandrakis, and Pohjolainen, 2011, for a recent review). The variation of the brightness temperature with frequency provides valuable data for modeling, while the circular polarization gives estimates of the magnetic field.

Owing to the limited spatial resolution, useful information can only be obtained with large radio telescopes or interferometers. The chromospheric network was first detected in interferometric data (Kundu and Velusamy, 1974; Kundu and Alissandrakis, 1975; Zirin, Hurford, and Marsh, 1978). The first, one-dimensional, imaging observations came from the *Radio Astronomical Telescope of the Academy of Sciences* 600 (RATAN-600) in the wavelength range of 2 – 4 cm, which showed small-scale brightness fluctuations across the quiet Sun (Bogod and Korolkov, 1975; Gelfreikh *et al.*, 1977; Bogod, 1978); this phenomenon was called *solar radiogranulation*. Thanks to the high spatial resolution (9″ by 50″) at the wavelength of 1.35 cm, it was possible to identify the individual elements of the radiogranulation with bright and dark elements of the chromospheric network visible in the Ca II K line (Gelfreikh *et al.*, 1982). In the millimeter range, small-scale structures (SSS) were first observed during the passage of Mercury across the disk of the Sun with the *Radio Telescope 22* (RT-22) (Efanov, Moiseev, and Severnyi, 1975) and with the *Radio Telescope 25* RT-25 by Kisliakov *et al.* (1975). Gelfreikh *et al.* (1982) made a comparison with optical images. Typical sizes of the cells obtained by Bogod (1978) and Gelfreikh *et al.* (1982) were 40″ to 50″ in the range from 1.96 cm to 10 cm.

Further observations with two-dimensional resolution came from synthesis instruments. Kundu *et al.* (1979) were the first to obtain quiet-Sun images at a wavelength of 6 cm with arcsecond resolution using the *Westerbork Synthesis Radio Telescope* (WSRT). The WSRT quiet-Sun images showed a clear association of the quiet-Sun microwave emission with the chromospheric network. This conclusion was subsequently verified with the *Very Large Array* (VLA) observations at 6 and 20 cm by Gary and Zirin (1988) and by Gary, Zirin, and Wang (1990) at 3.6 cm. In the mid-1990s the VLA was used for quiet-Sun observations in the short centimeter-range (1.2, 2.0 and 3.6 cm) by Bastian, Dulk, and Leblanc (1996), Benz *et al.* (1997), and Krucker *et al.* (1997). In addition to the chromospheric network, SSS are also associated with other features, such as X-ray bright points, ephemeral active regions, magnetic elements, and, possibly, with small coronal loops.

The chromospheric structure is of special interest as an input to the theories of coronal heating (Aschwanden *et al.*, 2007; Peter, Bingert, and Kamio, 2012; Zacharias, Peter, and Bingert, 2011; see also the review by Tsiropoula *et al.*, 2012). In recent years, significant advances have been made in the study of solar EUV emission with the *Hinode* instruments (Ji, Cao, and Goode, 2012), as well as the *Atmospheric Imaging Assembly* (AIA: Lemen *et al.*, 2012) telescopes onboard the *Solar Dynamic Observatory* (SDO: Pesnell, Thompson, and Chamberlin, 2012); but these instruments provide no information on the strength of the magnetic field.

To estimate the magnetic field at the level of the transition region and lower corona, we need to resort to radio observations with the large radio telescope RATAN-600, since the VLA does not have, up to now, sufficient sensitivity to provide accurate measurements of the low circular polarization in the quiet Sun. Although RATAN-600 has a lower resolution than the VLA or EUV instruments, its sensitivity is high enough to record the SSS in the microwave range. In recent years, a new multiwavelength spectral and polarization equipment has been installed in RATAN-600 (Bogod, 2011; Bogod, Alesin, and Pervakov, 2011), which has a spectral resolution of 1 % and a frequency range from 3 GHz to 18.2 GHz. This system uses a high-speed digital data acquisition system with a wide dynamic range, which provides a high signal-to-noise ratio from the level of the quiet Sun up to that of bursts, in many wavelengths simultaneously.

In this article we present the first results of a study of small-scale quiet-Sun structures in the microwave range during the time interval from September 2005 to July 2012, made with the RATAN-600 using its new technical capabilities. The observations and their analysis are described in Section 2; our results are presented in Section 3 and are discussed in Section 4.

2. Observations and Data Reduction

The observations were made in the southern sector of the antenna system with the periscopic mirror (Bogod *et al.*, 2004). In this configuration it is possible to make multiple observations at different azimuths. This provides scans along different position angles across the Sun (depending on the declination), together with extended time coverage. In 2012, the polarization characteristics of the receiving equipment were improved. The former spiral right and left circular polarization feeds, which were shifted from the focus, were replaced by wide-range sinus-type feeds that have a common phase center for both the right and left circular polarizations (Bogod, 2011). This eliminated wavelength-dependent aberrations caused by the shift from the focus.

The radio telescope has a large effective area (300 – 600 m^2) in the centimeter range. It provides a flux sensitivity of $\sim$0.01 sfu, with a position accuracy of about $1''$. It covers a broad frequency band with high spectral resolution, it has a relatively wide range of coverage in time (07:00 UT to 11:00 UT), and high-precision measurement of the polarized signal, 0.05 to 0.2 %.

In the early observations of quiet-Sun small-scale structures obtained with RATAN-600 (Bogod and Korolkov, 1975; Bogod, 1978), the antenna system of the northern sector was used; in this system the vertical size of the beam was only six times larger than the horizontal one. Since 2005, regular solar observations with RATAN-600 are made, using the southern sector with a periscopic mirror. The beam pattern has a knife-edge shape (for example, at 2 cm the beam size is $17''$ by $15'$). Assuming a uniform distribution of the network cells, a strong smoothing effect might be expected because at least 12 – 15 cells are included in the vertical beam pattern. However, as can be seen from Figures 1 and 2, the SSS is well depicted in the one-dimensional (1D) scans across a broad frequency range.

The digital multichannel data-recording system (Baldin and Garaimov, 2011) provides an increased dynamic range that extends from the instrumental noise level (antenna temperature of about 300 to 500 K) up to the high-power signals during flares (about 200 to 500×10^3 K). This corresponds to about 30 to 80 $\times T_a$, where T_a is the level of the quiet-Sun antenna temperature. To separate the quiet-Sun structures we used the following method:

i) Calibration of the multiwavelength data.
ii) Subtraction of the large-scale background component, including the quiet-Sun emission (Figure 3); this leaves some residual background emission near the limbs.
iii) Low-pass filtering to reduce small-scale noise with a characteristic angular size much smaller than the resolution.

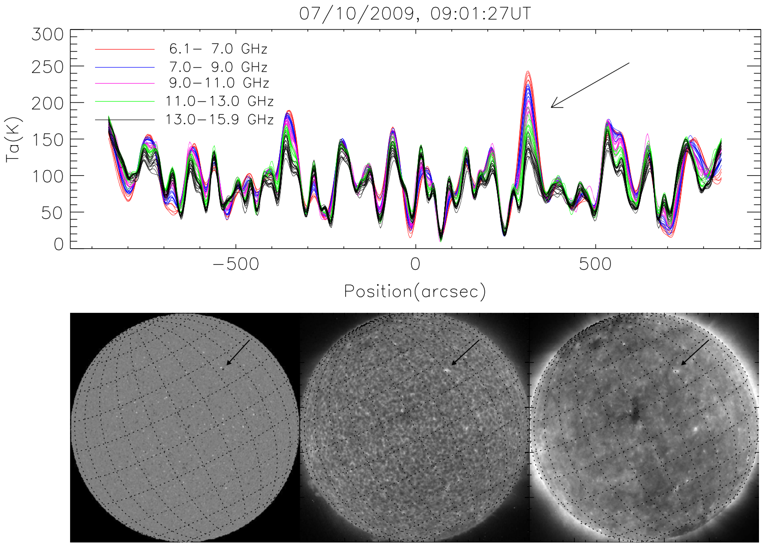

Figure 1 Example of multiwavelength 1D observations (scans) of the quiet Sun obtained with the RATAN-600 radio telescope on 7 October 2009 (top). In the bottom row we show from left to right images from the *Solar and Heliospheric Observatory* (SOHO) *Michelson Doppler Imager* (MDI), and the *Extreme ultraviolet Imaging Telescope* (EIT) at 304 Å and 171 Å oriented in the celestial EW-NS direction. The arrows mark the brightest source on the radio scans and the images.

3. Results

3.1. Temporal Characteristics

Observations at different azimuths allowed us to study the stability in time of the SSS. Figure 4 shows four-hour-long observations in 11 azimuths obtained on 14 March 2008, with a cadence of about 24 minutes. Note that these observations were taken near the time of the vernal equinox, so that the orientation of the scans with respect to the solar E–W direction is practically the same. Taking into account the rotation of the Sun, a high degree of correlation (> 82 %) is found between consecutive scans, and up to 60 % between observations separated by a few hours. Thus the SSS are a long-lived solar phenomenon, rotating with the Sun. The average brightness of the SSS is about $1-1.5$ % of that of the quiet Sun.

3.2. Comparison of RATAN-600 Data with SDO/AIA Data

To localize the radio structures on the disk, we compared the RATAN-600 1D scans with optical and EUV images. After the new polarization feeds were installed (see Section 2), solar activity was close to its maximum, therefore there were only few days devoid of active regions. For our analysis we selected the date of 5 February 2012, when the SSS were well visible, even though an active region was present near the west limb (Figure 5).

The SDO provides the best set of images for comparison with the RATAN-600 data. They have a high cadence, which permitted us to select images very close to the RATAN-600 observations, and they cover a wide range of heights from the chromosphere to the low corona. The first step in the comparison was the convolution of the SDO images with the RATAN-600 beam. Subsequently, we removed large-scale structure in the E–W direction

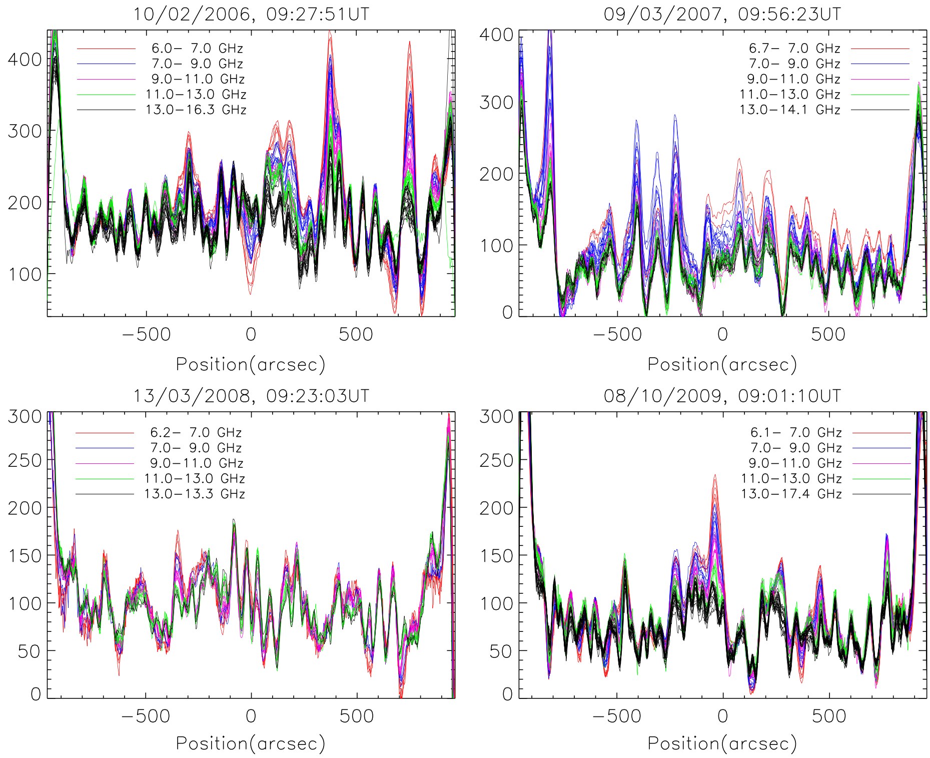

Figure 2 Examples of recordings of solar SSS in the range of 6 to 18 GHz during the period of solar activity minimum, 2005 to 2009. The intensity scans are shown after subtracting the large-scale background component. Scans in several wavelengths in the range of 6 – 16.4 GHz are presented. The variations are 0.01 to 0.03 of the quiet-Sun antenna temperature.

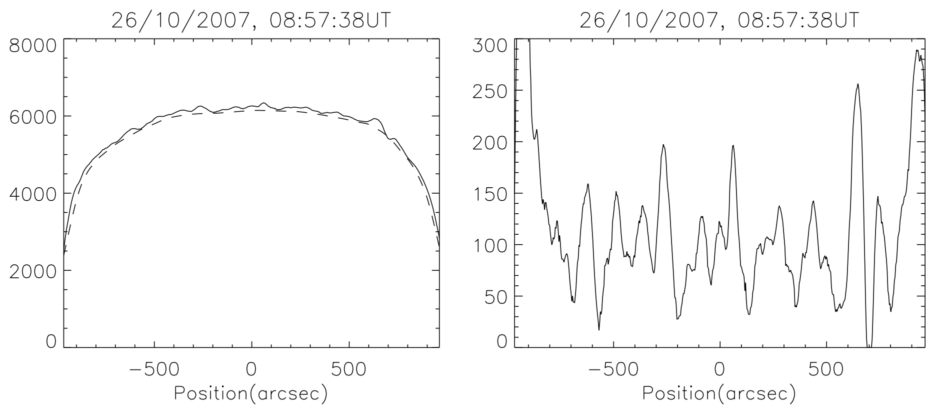

Figure 3 Large-scale component subtraction to enhance small-scale structures. The left panel shows the original scan and the background component (dashed line), while the right panel shows the residual structure after the subtraction.

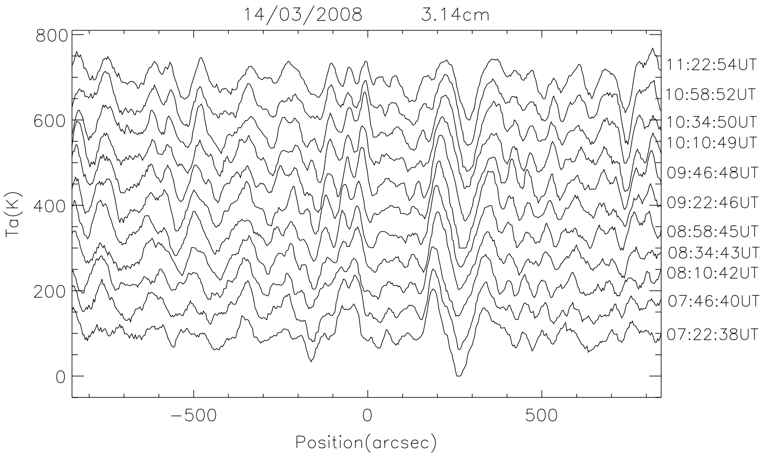

Figure 4 Changes in the SSS during 4 hours, from observations at different azimuths. The time interval between consecutive scans is 24 minutes. The gradual drift of the sources to the right is due to the solar rotation.

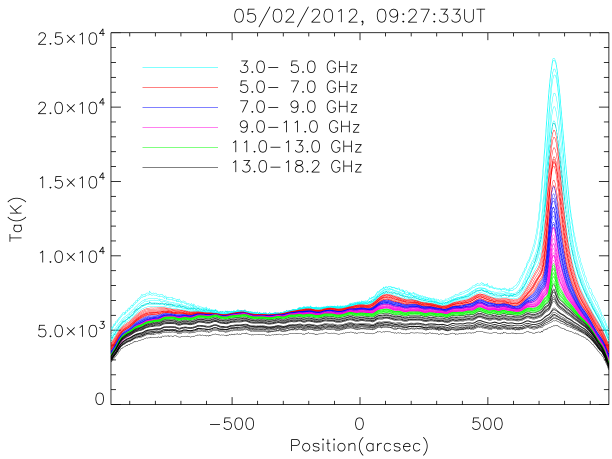

Figure 5 Multifrequency RATAN-600 1D solar scans for 5 February 2012.

by high-pass filtering with a Gaussian of 60″ width. Figure 6 shows in the left column the original SDO images in selected SDO bands, the middle column shows the same images convolved with the instrumental beam at the shortest wavelength (1.65 cm), while the result of the high-pass filtering is shown in the right column. Note that small-scale structures persist despite the smoothing with the RATAN-600 beam.

The comparison of the two data sets is complicated by the change of the RATAN-600 resolution, as well as possible changes of the radio structures as a function of wavelength because of the change of the opacity and the subsequent change of formation height. To avoid the problem with the change of resolution, we simulated the effect of the RATAN-600 beam on the SDO images. In the images shown in Figure 7, each row is the convolution of an SDO image by the radio beam at a particular frequency; thus, they simulate what SDO would observe if it operated in the same way as RATAN-600. These images are directly comparable with images of the RATAN-600 antenna temperature as a function of position

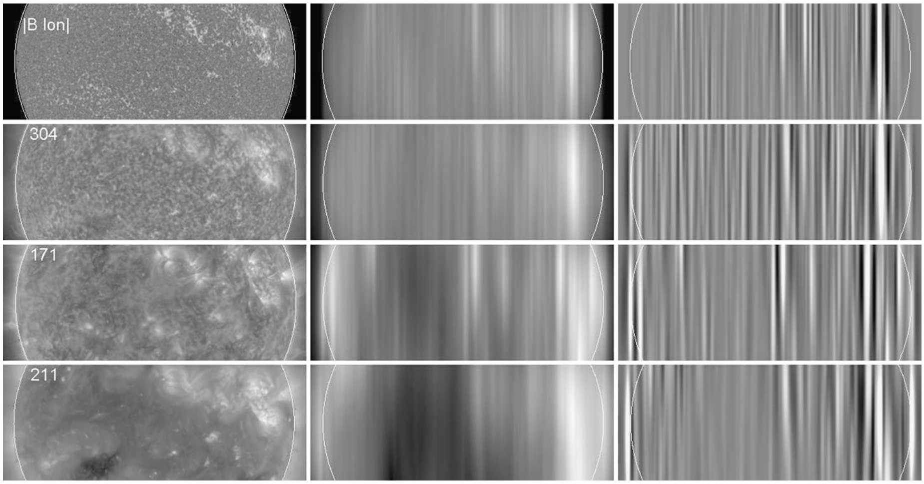

Figure 6 Left column: original SDO images for 5 February 2012 (from top to bottom: absolute value of the longitudinal magnetic field from the *Helioseismic and Magnetic Imager*, and images in 304, 171, and 211 Å bands from AIA). Central column: similar to the left column, after convolution with the RATAN-600 beam pattern at 1.65 cm. Right column: the result of high-pass filtering in the E–W direction. The images are centered on the disk center and are oriented in the celestial E–W and N–S direction. The size of the region shown is 2100″ by 800″. White arcs mark the photospheric limb.

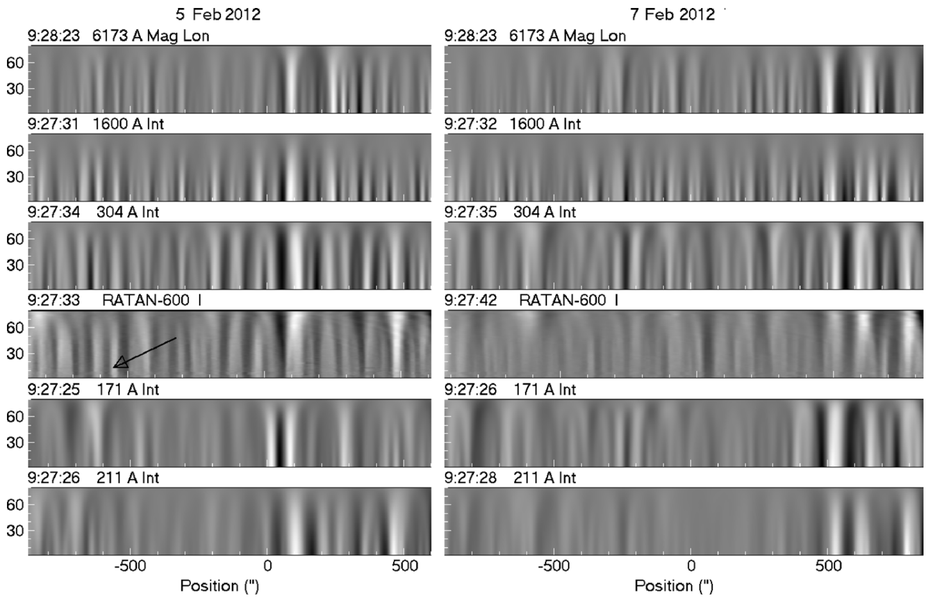

Figure 7 Comparison of images of the RATAN-600 antenna temperature as a function of position and frequency with simulated SDO images ($|B_\ell|$, intensity in the 1600, 304, 171, and 211 Å bands), for 5 February (left) and 7 February 2012 (right). The range of positions was selected such as to avoid the active region near the west limb. The ordinate is the frequency channel, which is almost linear in frequency with channel 1 at 18.2 GHz (1.65 cm) and channel 80 at 3 GHz (10 cm). The arrow in the RATAN-600 data of 5 February points at the feature analyzed in Section 3.3.

Table 1 Cross-correlation between RATAN-600 and SDO data.

Band	5 February	7 February
$\|B_\ell\|$	0.34	0.23
1600	0.58	0.64
304	0.71	0.74
171	0.25	0.52
193	0.31	0.63
211	0.43	0.64
131	0.18	0.61
335	0.46	0.68
94	0.36	0.66

and frequency, also shown in Figure 7. The RATAN-600 data were also subjected to high-pass filtering for consistency with the SDO data. In addition to the 5 February 2012 data, we also present data for 7 February.

The similarity of the RATAN-600 data to the SDO data is striking, particularly in the 1600 and 304 Å bands; there is practically a peak-to-peak correspondence in the entire frequency range for both days. To obtain a more quantitative result, we computed the cross-correlation coefficient between the antenna temperature at each radio frequency and the corresponding SDO simulated scan. The average for all frequencies is given in Table 1.

The results show that the highest correlation of the radio data is with the 304 Å band (0.71 and 0.74 for February 5 and 7 respectively), formed in the low transition region at a temperature of about 10^5 K. The next-highest correlation is with the 1600 Å band (0.58 and 0.64), formed in the low chromosphere. The correlation with the absolute value of the longitudinal magnetic field, $|B_\ell|$, is relatively low, probably because the radio emission is related to the absolute value of the magnetic field and not to its longitudinal component. We note, for comparison, that the correlation between the 304 Å band and the $|B_\ell|$ images is low as well; its value is 0.44 and 0.34 for the two days considered. The correlation decreases significantly toward the 171 Å band, formed in the middle to upper transition region (at $\sim 10^6$ K). There is a slight increase of the correlation with the SDO bands formed in the low corona, but this is probably caused by the plage and not by the quiet-Sun component of the emission; indeed, as can be seen in Figure 7, most microwave features in the eastern hemisphere, which is devoid of plage regions, are not visible in the 211 Å band.

The identification of the peaks seen in the 1D scans with solar features presents inherent difficulties because of the confusion introduced by the integration in the N–S direction. Such a comparison is shown in Figure 8, where the RATAN-600 positional-spectral image and the corresponding AIA 304 Å simulated image (*cf.* Figure 7) are shown, together with the original 304 Å and B_ℓ images. In addition to the active region near the limb, the comparison shows a number of cases, marked by ellipses in the 304 Å image, where the SSS peaks are associated with spotless plage or small bipolar regions. In most cases, however, there is no clear association of the peaks with distinct structures either in the 304 Å image or in B_ℓ. Apparently, such peaks are the sum of several individual structures.

3.3. Spectral Properties of the SSS

We investigated the spectral properties of an individual peak, marked with the arrow in Figure 7, using a least-squares fit of the antenna temperature profile with a Gaussian model

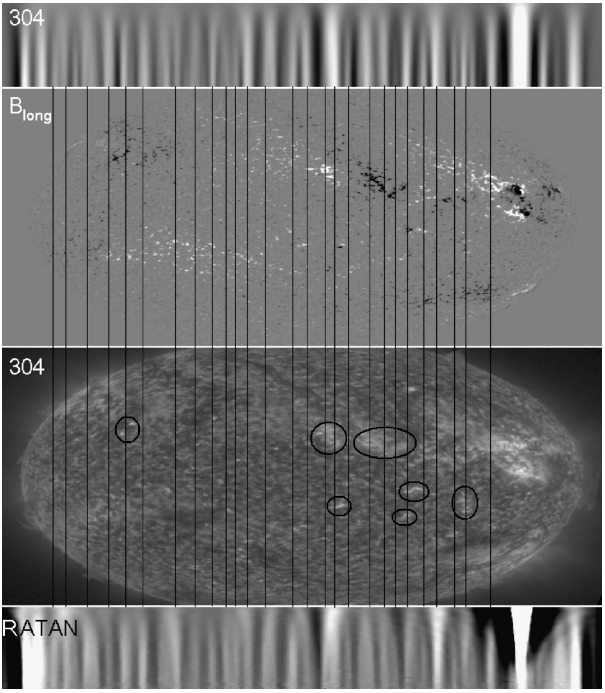

Figure 8 Comparison of the RATAN-600 position–frequency data (bottom) of 5 February 2012 with the AIA image in the 304 Å band and the HMI image of B_ℓ, both compressed in the N–S direction. For reference, the top panel shows the 304 Å data in a form simulating the RATAN data. Vertical lines mark the 1D position of the SSS peaks.

(Garaimov, 1997). In this way, we measured the flux, the size, the brightness temperature and the position of the feature as a function of frequency (Figure 9). Note that we were unable to reliably compute the brightness temperature below 11 GHz.

The flux density of this feature demonstrates a clear steady increase with frequency, which stabilizes around 12 GHz (2.5 cm). The size decreases from about 30″ at low frequencies to about 20″ at high frequencies; this variation is probably due to the combined effect of the change of instrumental resolution and real structural changes, as mentioned previously. The brightness temperature shows little change at high frequencies (from 18 to 13 GHz, 1.7 to 2.3 cm), with a value of about 20×10^3 K. Subsequently it increases to about 70×10^3 K at 11 GHz. This increase might be due to the shift of the level of formation of the radiation into the low transition region. The position of the peak is constant in most of the frequency range, but below 6 GHz shifts eastward (see also Figure 7). This might be due to the loss of resolving power at low frequencies and subsequent merging with other peaks.

A more global estimate of the characteristic size is provided by the width of the autocorrelation function in the spatial domain. Our computations (Figure 10) give an autocorrelation width of 25″ to 30″ at 1.65 cm, increasing at longer wavelengths to $\sim$50″; these values are consistent with those quoted in the previous paragraph. At shorter wavelengths the increase of the width is almost linear, as expected for a structure smaller than the beam size; however, above $\sim$7.5 cm the value of the width stabilizes. This is also seen in Figure 7, and it probably reflects a real change in structure, apparently caused by the rise of the formation level of the radiation.

3.4. Polarization and Estimate of the Magnetic Field of Individual Features

It is interesting to obtain estimates of the magnetic field at altitudes of the lower corona, using polarization observations of the SSS. In Figure 11 multiwavelength observations of

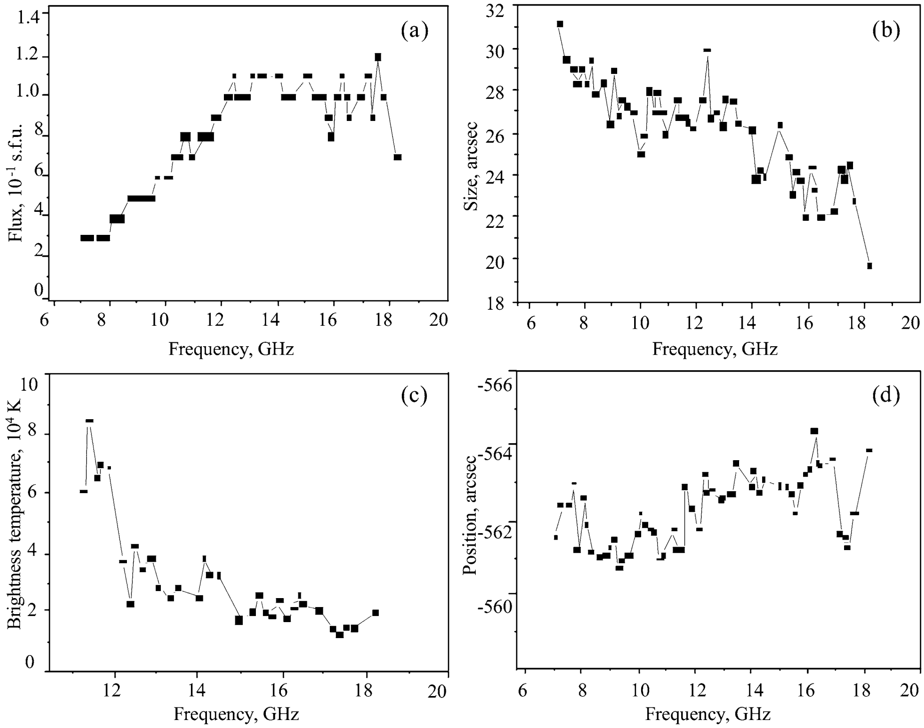

Figure 9 The flux (a), the size (b), the brightness temperature (c), and the position (d) of the feature marked by the arrow in Figure 7 as a function of frequency.

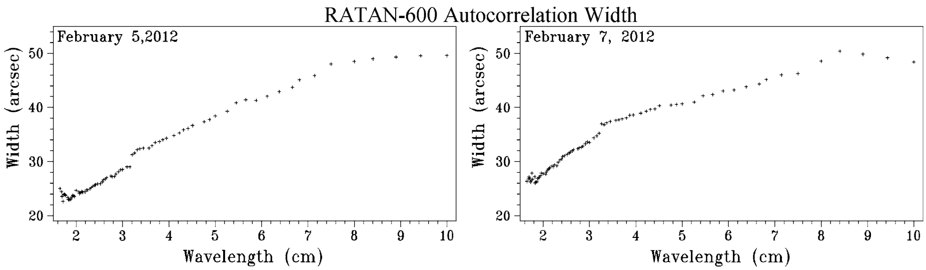

Figure 10 The width of the autocorrelation function as a function of frequency.

the SSS in Stokes parameters I and V are shown for 8 February 2012, processed as described above. We note that the polarized radiation is above the background noise, higher than the $\pm 3\sigma$ level. The estimated highest value of the degree of polarization is about $4-5$ %.

To analyze the properties of SSS polarized emission we used the observations in the $\lambda = 2$ cm scan of 8 February 2012 (Figure 12). Seven radio structures were selected whose polarized signal exceeded the 3σ confidence level. Table 2 gives the values of the polarization degree and the magnetic field, computed under the assumption of thermal free–free emission and homogeneous magnetic field; in this case the magnetic field is

$$B = 5400 p/\lambda,$$

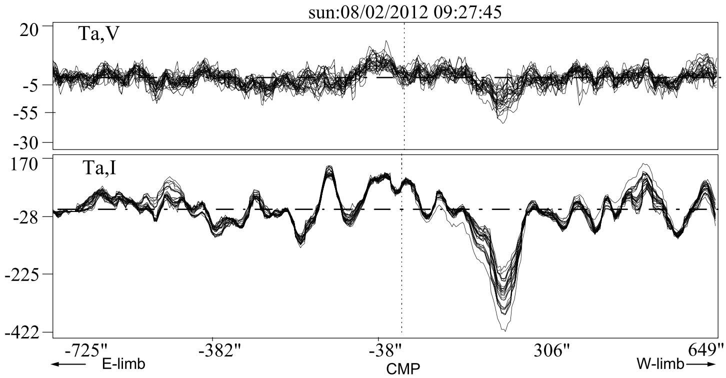

Figure 11 Stokes V (top) and I (bottom) data for 8 February 2012 in the wavelength range of 1.82 to 3.26 cm at 27 frequencies. The antenna temperature scale of the V plot is expanded by a factor of 10.

Figure 12 Analysis of several individual structures in the 2 cm scan. The ellipses mark the sources for which the magnetic field was computed.

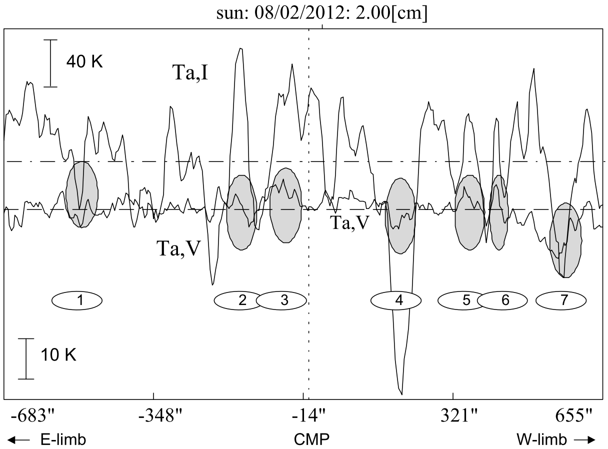

Table 2 Polarization degree and computed magnetic field for the structures marked in Figure 12.

No.	1	2	3	4	5	6	7
P (%)	3.75	2.5	5.8	1.4	6.25	8.5	7.1
B (G)	100	67	155	37	170	230	190

where $p = V/\Delta I$ is the degree of polarization, ΔI is the intensity difference with respect to the background, and λ is the wavelength in cm. The obtained values of the magnetic field, which are in the range of 40 to 200 Gauss, should be considered as a weighted average because of the integration within the instrumental beam.

4. Summary and Conclusions

In spite of the large width of the RATAN-600 beam in the N–S direction, small-scale structures are detected in the 1D scans in the wavelength range of 1.65 to 10 cm. The sensitivity of the instrument is sufficient to detect flux variations of ~ 0.01 sfu. The SSS, with a brightness of 1 to 3 % above the quiet-Sun level, are stable over several hours, with a characteristic timescale of about one day. Their observed characteristic size increases with wavelength from about $25''$ to about $50''$, as the resolution decreases; above ~ 7.5 cm the characteristic size stabilizes, which might be an indication of a real structural change.

A comparison of the microwave SSS with SDO images, treated in a way that simulates the behavior of RATAN-600, showed an almost one-to-one correspondence between the microwave structures and those seen in the 304 Å AIA band, with a somewhat inferior correlation with the 1600 Å AIA band. The correlation with the 171 Å band was weak, therefore we conclude that the radio SSS emission comes from a region extending from the chromosphere to the low transition region and does not extend to the height of formation of the 171 Å band, which has its peak sensitivity near a temperature of 6.3×10^5 K.

The exact identification of the SSS with particular structures proved to be extremely difficult, except in the case of patches of old plage and some intense bipolar regions. The rest of the features appear to be due to the merging of several individual structures of the chromospheric network that exist within the instrumental beam.

Our results agree with the conclusion of previous observations (summarized by Shibasaki, Alissandrakis, and Pohjolainen, 2011), as far as the association of radio structures with the chromospheric network is concerned, moreover, we covered here a more extended frequency range than previous observations. As for the network itself, it is well-known from EUV data that it becomes diffuse in the upper transition region and disappears in the low corona; for example, there is no trace of the network in SDO images in the 171 Å band. A similar behavior is expected for the radio network, and our results are consistent with this.

In addition to the association of radio SSS with EUV structures, RATAN-600 data provided measurements of the circular polarization and hence of the magnetic field. Our estimates of 40 to 200 Gauss should be considered as a weighted average because of the integration over the instrumental beam.

Although the spatial resolution of our data is much inferior to that obtained by modern instruments operating in the EUV, RATAN-600 observations of SSS have certain merits that we would like to emphasize. The most important one is the possibility to estimate the magnetic field, which is still beyond the capability of EUV instruments. Moreover, the complete spectral coverage of the RATAN-600, which extends over a frequency range with $f_{\max}/f_{\min} \sim 6$, is an extremely useful input to detailed modeling of the solar atmosphere from the upper chromosphere to the low corona, where the microwave emission is formed. We note in this context that very little use has been made of the microwave fine-structure data in multicomponent atmospheric models (*cf.* Chiuderi Drago, Kundu, and Schmahl, 1983). It goes without saying that the interpretation of thermal radio emission is devoid of effects such as abundances, excitation, and ionization equilibria, which plague the interpretation of EUV data.

The new radio facilities currently under development will certainly add to our understanding of the physics of the network and its extent into the upper layers of the solar atmosphere. In particular, accurate polarization measurements will be possible with the *Jansky Very Large Array*, while the *Atacama Large Millimeter/submillimeter Array* (ALMA) is expected to extend our vision to the submm range (*cf.* White, Loukitcheva, and Solanki, 2006). The multifrequency version of the *Siberian Solar Radio Telescope* (SSRT), currently under development (see Kochanov *et al.*, 2013), is expected to provide two-dimensional spectral information. Last but not least, the *Expanded Owens Valley Solar Array* will provide a wide frequency coverage, although with a limited number of baselines and, moreover, it will be an instrument dedicated to solar research. Unfortunately, the ultimate solar radio instrument, the *Frequency Agile Solar Radiotelescope* (FASR), is still far from being realized.

The observed fine structure of the quiet Sun in microwaves apparently reflects manifestations of plasma inhomogeneities in the form of supergranulation or chromospheric network. This is indicated by their characteristic dimensions and lifetimes (Paniveni *et al.*, 2005). As suggested by many authors, the transformation of the magnetic energy into thermal energy may occur in the chromosphere. The main candidate here might be magnetic reconnection as the most efficient mechanism both for the release of energy into the corona and the transfer of cool plasma from the chromosphere to the corona (Tsiropoula *et al.*, 2012; Zacharias, Peter, and Bingert, 2011). Aschwanden *et al.* (2007) provided evidence that the heating takes place in the transition region and upper chromosphere, rather than in the corona. One of the main problems here is the magnetic complexity in the transition region, which makes it very difficult to trace the magnetic connectivity from coronal loops down to the photosphere (Jendersie and Peter, 2006).

Future work on fine structures in the chromosphere and low transition region with large optical and ultraviolet telescopes, as well as observations of fine radio structure in microwaves with radio telescopes with a large surface area will improve our understanding of their physics and dynamics. RATAN-600 provides a large data base of such observations, an extended frequency range, and the capability of measuring circular polarization. Therefore, it can contribute much to the research of these phenomena.

References

Aschwanden, M.J., Winebarger, A., Tsiklauri, D., Peter, H.: 2007, *Astrophys. J.* **659**, 1673.
Baldin, S.V., Garaimov, V.I.: 2011, *Astrophys. Bull.* **66**, 371.
Bastian, T.S., Dulk, G.A., Leblanc, Y.: 1996, *Astrophys. J.* **473**, 539.
Benz, A.O., Krucker, S., Acton, L.W., Bastian, T.S.: 1997, *Astron. Astrophys.* **320**, 993.
Bogod, V.M.: 1978, *Soobshchen. Spetsial. Astrofiz. Obs.* **23**, 22.
Bogod, V.M.: 2011, *Astrophys. Bull.* **66**, 190.
Bogod, V.M., Alesin, A.M., Pervakov, A.A.: 2011, *Astrophys. Bull.* **66**, 205.
Bogod, V.M., Korolkov, D.V.: 1975, *Sov. Astron. Lett.* **1**, 205.
Bogod, V.M., Zhekanis, G.N., Mingaliev, M.G., Tokhchukova, S.K.: 2004, *Radiophys. Quantum Electron.* **47**, 227.
Chiuderi Drago, F., Kundu, M.R., Schmahl, E.J.: 1983, *Solar Phys.* **85**, 237.
Efanov, V.A., Moiseev, I.G., Severnyi, A.B.: 1975, *Izv. Ord. Trud. Krasn. Znamen. Krym. Astrofiz. Obs.* **53**, 121.
Garaimov, V.I.: 1997, *Spec. Astrophys. Obs. Russ. Acad. Sci.* **27**, 1.
Gary, D.E., Zirin, H.: 1988, *Astrophys. J.* **329**, 991.
Gary, D.E., Zirin, H., Wang, H.: 1990, *Astrophys. J.* **355**, 321.
Gelfreikh, G.B., Bogod, V.M., Korzhavin, A.N., Smirnova, O.B., Startsev, S.V., Kononovich, E.V., Smirnova, O.B., Startsev, S.V., Piotrovich, V.V.: 1982, In: Fricke, W., Teleki, G. (eds.) *Astrophys. Space Scien. Lib.* **96**, Reidel, Dordrecht, 109.
Gelfreikh, G.B., Kaidanovskii, M.N., Kononovich, E.V., Smirnova, O.B., Stotskii, A.A., Trushkin, S.A.: 1977, *Sov. Astron. Lett.* **3**, 300.
Jendersie, S., Peter, H.: 2006, *Astron. Astrophys.* **460**, 901.
Ji, H., Cao, W., Goode, P.R.: 2012, *Astrophys. J. Lett.* **750**, L25.
Kisliakov, A.G., Kulikov, I.I., Fedoseev, L.I., Chernyshev, V.I.: 1975, *Sov. Astron. Lett.* **1**, 79.
Kochanov, A.A., Anfinogentov, S.A., Prosovetsky, D.V., Rudenko, G.V., Grechnev, V.V.: 2013, *Publ. Astron. Soc. Japan* **65**, 19.
Krucker, S., Benz, A.O., Bastian, T.S., Acton, L.W.: 1997, *Astrophys. J.* **488**, 499.
Kundu, M.R., Alissandrakis, C.E.: 1975, *Mon. Not. Roy. Astron. Soc.* **173**, 65.
Kundu, M.R., Rao, A.P., Erskine, F.T., Bregman, J.D.: 1979, *Astrophys. J.* **234**, 1122.
Kundu, M.R., Velusamy, T.: 1974, *Solar Phys.* **34**, 125.
Lemen, J.R., Title, A.M., Akin, D.J., Boerner, P.F., Chou, C., Drake, J.F., Duncan, D.W., Edwards, C.G., Friedlaender, F.M., Heyman, G.F., Hurlburt, N.E., Katz, N.L., Kushner, G.D., Levay, M., Lindgren, R.W., Mathur, D.P., McFeaters, E.L., Mitchell, S., Rehse, R.A., Schrijver, C.J., Springer, L.A., Stern, R.A., Tarbell, T.D., Wuelser, J.-P., Wolfson, C.J., Yanari, C., Bookbinder, J.A., Cheimets, P.N., Caldwell,

D., Deluca, E.E., Gates, R., Golub, L., Park, S., Podgorski, W.A., Bush, R.I., Scherrer, P.H., Gummin, M.A., Smith, P., Auker, G., Jerram, P., Pool, P., Soufli, R., Windt, D.L., Beardsley, S., Clapp, M., Lang, J., Waltham, N.: 2012, *Solar Phys.* **275**, 17.
Paniveni, U., Krishan, V., Singh, J., Srikanth, R.: 2005, *Solar Phys.* **231**, 1.
Pesnell, W.D., Thompson, B.J., Chamberlin, P.C.: 2012, *Solar Phys.* **275**, 3.
Peter, H., Bingert, S., Kamio, S.: 2012, *Astron. Astrophys.* **537**, A152.
Shibasaki, K., Alissandrakis, C.E., Pohjolainen, S.: 2011, *Solar Phys.* **273**, 309.
Tsiropoula, G., Tziotziou, K., Kontogiannis, I., Madjarska, M.S., Doyle, J.G., Suematsu, Y.: 2012, *Space Sci. Rev.* **169**, 181.
White, S.M., Loukitcheva, M., Solanki, S.K.: 2006, *Astron. Astrophys.* **456**, 697.
Zacharias, P., Peter, H., Bingert, S.: 2011, *Astron. Astrophys.* **532**, A112.
Zirin, H., Hurford, G.J., Marsh, K.A.: 1978, *Astrophys. J.* **224**, 1043.